Neurosci. Bull. August, 2019, 35(4):649–660
https://doi.org/10.1007/s12264-019-00351-2

www.neurosci.cn
www.springer.com/12264

ORIGINAL ARTICLE

Comparative Study of ROCK1 and ROCK2 in Hippocampal Spine Formation and Synaptic Function

Jinglan Yan[1] · Youcan Pan[1,3] · Xiaoyan Zheng[1] · Chuanan Zhu[1] · Yu Zhang[1] · Guoqi Shi[1] · Lin Yao[2] · Yongjun Chen[1,4] · Nenggui Xu[1]

Received: 29 July 2018 / Accepted: 23 November 2018 / Published online: 2 March 2019

Abstract Rho-associated kinases (ROCKs) are serine-threonine protein kinases that act downstream of small Rho GTPases to regulate the dynamics of the actin cytoskeleton. Two ROCK isoforms (ROCK1 and ROCK2) are expressed in the mammalian central nervous system. Although ROCK activity has been implicated in synapse formation, whether the distinct ROCK isoforms have different roles in synapse formation and function *in vivo* is not clear. Here, we used a genetic approach to address this long-standing question. Both Rock1$^{+/-}$ and Rock2$^{+/-}$ mice had impaired glutamatergic transmission, reduced spine density, and fewer excitatory synapses in hippocampal CA1 pyramidal neurons. In addition, both Rock1$^{+/-}$ and Rock2$^{+/-}$ mice showed deficits in long-term potentiation at hippocampal CA1 synapses and were impaired in spatial learning and memory based on the water maze and contextual fear conditioning tests. However, the spine morphology of CA1 pyramidal neurons was altered only in Rock2$^{+/-}$ but not Rock1$^{+/-}$ mice. In this study we compared the roles of ROCK1 and ROCK2 in synapse formation and function *in vivo* for the first time. Our results provide a better understanding of the functions of distinct ROCK isoforms in synapse formation and function.

Keywords Rho-associated kinases · Spine · Hippocampus · STP · LTP · Spatial learning and memory

Introduction

The actin cytoskeleton is critical for the regulation of dendritic spines and synaptic function [1–3], and the Rho-associated coiled-coil-containing kinases (ROCKs) are potent regulators of the actin cytoskeleton. There are two mammalian ROCK isoforms, ROCK1 and ROCK2; the full-length proteins share 64% amino-acid similarity and the kinase domains share 83% identity [4]. ROCKs have been shown to be crucial for spine formation and synaptic function [5–8]. However, the roles of ROCKs in synapse formation and function are controversial. Y-27632, a pan-ROCK inhibitor, has been reported to increase spine density and reduce spine width without affecting spine length in cultured hippocampal neurons [9]. By contrast, cultured hippocampal neurons from Rock2$^{+/-}$ mice show normal spine density but increased spine length compared with control neurons [10]. Therefore, it is challenging to assign functions to ROCK1 and ROCK2 based on inhibitor

Jinglan Yan, Youcan Pan and Xiaoyan Zheng have contributed equally to this work.

Electronic supplementary material The online version of this article (https://doi.org/10.1007/s12264-019-00351-2) contains supplementary material, which is available to authorized users.

✉ Yongjun Chen
ychen@gzucm.edu.cn

✉ Nenggui Xu
ngxu8018@163.com

1 South China Research Center for Acupuncture and Moxibustion, Medical College of Acu-Moxi and Rehabilitation, Guangzhou University of Chinese Medicine, Guangzhou 510006, China

2 School of Pharmaceutical Sciences, Guangzhou University of Chinese Medicine, Guangzhou 510006, China

3 Guangdong Provincial Hospital of Chinese Medicine, Guangzhou 510006, China

4 Guangdong Province Key Laboratory of Psychiatric Disorders, Southern Medical University, Guangzhou 510515, China

studies because the current ROCK inhibitors are not isoform-specific and likely have off-target effects.

Although ROCK1 and ROCK2 share downstream substrates such as myosin phosphatase target subunit 1, myosin light chain (MLC), and LIM kinases, evidence from genetic studies suggests that ROCK isoforms have distinct functions [11–15]. Using Rock1$^{-/-}$ and Rock2$^{-/-}$ mouse embryonic fibroblasts, Shi *et al.* demonstrated different roles of ROCK1 and ROCK2 in regulating the actin cytoskeleton: ROCK1 destabilizes actin through MLC phosphorylation, whereas ROCK2 stabilizes actin *via* cofilin phosphorylation [16]. These studies suggest that ROCK1 and ROCK2 have distinct functions *in vitro*. However, investigation of the roles of ROCK isoforms *in vivo* is hampered by developmental defects in Rock1$^{-/-}$ and embryonic lethality in Rock2$^{-/-}$ mice [17–19].

Despite the fact that Rock1$^{+/-}$ and Rock2$^{+/-}$ mice develop normally, *in vivo* studies on spine formation and synapse function using these heterozygous models are rare. Zhou *et al.* showed that the synapse number, glutamatergic transmission, and long-term potentiation (LTP) in the hippocampus are impaired in Rock2$^{-/-}$ mice [10]. However, whether Rock2$^{+/-}$ mice are also deficient in hippocampus-dependent behaviors remains to be determined, and studies on spine formation and synaptic function in Rock1$^{+/-}$ mice are lacking.

Therefore, in this study, we investigated the spine density, morphology, and synaptic function in the hippocampus of Rock1$^{+/-}$ and Rock2$^{+/-}$ mice with the same genetic background.

Materials and Methods

Animals

The Rock1$^{+/-}$ and Rock2$^{+/-}$ mice were gifted from Dr. Robert W. Caldwell of Augusta University, Georgia, USA and maintained on a C57BL/6J genetic background [20]. Mice were housed at 25°C under a 12-h light/dark cycle, and food and water were available *ad libitum*. The genotyping primers for Rock1$^{+/-}$ mice were as follows: forward: 5′ AGG CAG GGC TAC ACA GAG AA 3′; reverse: 5′ ACA GCT GCC ATG GAG AAA AC 3′. The PCR products for the wild-type (WT) and Rock1$^{+/-}$ alleles were 918 bp and 544 bp, respectively. The genotyping primers for Rock2$^{+/-}$ mice were as follows: forward: 5′ GTT TCT CAG CAT TAT GTT GG 3′ and 5′ CTG GGT TGT TTC TCA GAT GA 3′; reverse: 5′ CGC TTT CAT CTG TAA ACC TC 3′. The PCR products for the WT and Rock2$^{+/-}$ alleles were 1 kb and 800 bp, respectively. To avoid influence of the hormonal cycle in female mice, all experiments were performed using 2–3 month-old male mice. All experimental procedures were reviewed and approved by the Institutional Animal Care and Use Committee of Guangzhou University of Chinese Medicine.

Western Blot

Western blot analysis was performed as described in our previous studies [21]. Homogenates of cerebral cortex and hippocampus were prepared in RIPA Buffer (in mmol/L: 50 Tris-HCl pH 7.4, 150 NaCl, 2 EDTA, 1 PMSF, 50 NaF, 1 sodium vanadate, 1 DTT, 1% sodium deoxycholate, 1% SDS, and protease inhibitor cocktail). The homogenates were resolved on SDS/PAGE gels and transferred to nitrocellulose membranes, which were incubated in TBS buffer containing 0.1% Tween-20 and 5% milk for 1 h at room temperature, then incubated with primary antibody overnight at 4 °C. After washing, the membranes were incubated with HRP-conjugated secondary antibody in the same TBS buffer for 1 h at room temperature. Immunoreactive bands were visualized using enhanced chemiluminescence (Pierce Biotechnology, Waltham, MA). Films were scanned with an Automatic Gel Imaging Analysis System (Peiqing Science and Technology, Shanghai, China) and analyzed with ImageJ (NIH, Washington, USA). The following antibodies were used: primary antibodies against ROCK1 (1:500; Abcam, Shanghai, China; ab45171), ROCK2 (1:2000; BD Biosciences, San Diego, CA; 610623), and GAPDH (1:2000; Abcam; ab8245) and secondary antibodies against mouse (1:3000; Abcam; ab6728).

Golgi Staining

Golgi staining was performed using a kit following the manufacturer's protocol (FD NeuroTechnologies, Columbia, SC). Three independent coronal sections (100 μm) containing the dorsal hippocampus (Bregma − 1.70 mm to −2 .46 mm) were imaged per mouse. Spines were counted on the secondary and tertiary branches of apical dendrites in the stratum radiatum of the hippocampal CA1 region. A 10-μm segment of either secondary or tertiary dendrite from pyramidal neurons in the CA1 region of the hippocampus was randomly selected in each section. All segments were observed under a Nikon Eclipse E400 microscope (Tokyo, Japan) by an investigator blind to the genotype. Spine density was calculated as described by Gibb and Kolb [22]; spines on secondary dendrites were visualized using a 100 × oil-immersion lens, and the number of spines along a 10-μm segment was counted to determine the number of spines/μm.

Electron Micrograph

The mice were sacrificed and the hippocampus CA1 tissue was sampled after cardiac perfusion with a mixture of 0.2% glutaraldehyde and 4% paraformaldehyde. The tissue was cut into ~ 1 mm^3 pieces, and fixed in 2.5% glutaraldehyde at 4 °C for 6 h. After fixing with 1% osmium tetroxide for 1 h and ethanol dehydration, the tissue was embedded in epoxy resin and prepared for ultrathin sectioning. Ultrathin sections were examined in an H-7650 transmission electron microscope (Hitachi, Tokyo, Japan). Excitatory/asymmetric synapses were identified by ultrastructural specializations, including a postsynaptic density (PSD), a wide synaptic cleft, and round synaptic vesicles. For each genotype, a total of 90 images were analyzed. The synapse density was calculated as the total number of synapses divided by the total volume of the section. The length and thickness of PSDs were analyzed using ImageJ (NIH).

Electrophysiology

Mice were anesthetized with ether and perfused transcardially for 1 min with 4 °C modified artificial cerebrospinal fluid (ACSF) containing (in mmol/L) 250 glycerol, 2 KCl, 10 $MgSO_4$, 0.2 $CaCl_2$, 1.3 NaH_2PO_4, 26 $NaHCO_3$, and 10 glucose to protect central nervous system neurons and maintain functional connectivity in the brain slices. The mice were then decapitated and brains were quickly removed and chilled in ice-cold ACSF for an additional 1 min. Transverse hippocampal slices (300 μm) were prepared using a Vibroslice (VT 1200S; Leica, Nussloch, Germany) in ice-cold ACSF. The slices were then incubated in regular ASCF containing (in mmol/L) 126 NaCl, 3 KCl, 1.25 NaH_2PO_4, 1.0 $MgSO_4$, 2.0 $CaCl_2$, 26 $NaHCO_3$, and 10 glucose for 30 min at 34 °C for recovery, and then at room temperature (25 ± 1 °C) for an additional 2–8 h. All solutions were saturated with 95% O_2/5% CO_2 (*v*/*v*).

Slices were placed in a recording chamber perfused (3 mL/min) with ACSF at 32–34 °C. Whole-cell voltage clamp recordings were made from hippocampal CA1 pyramidal neurons. Patch electrodes (3–7 MΩ) were filled with a solution containing (in mmol/L) 105 K-gluconate, 30 KCL, 10 HEPES, 10 phosphocreatine, 4 ATP-Mg, GTP-Na, and 0.3 EGTA, pH 7.35, 285 mOsm. To measure the miniature excitatory postsynaptic currents (mEPSCs), voltage clamp recordings were performed at − 70 mV in the presence of 1 μmol/L TTX and 20 μmol/L bicuculline. Field excitatory postsynaptic potentials (fEPSPs) were evoked in the CA1 stratum radiatum by stimulating the Schaffer collaterals with a concentric bipolar electrode (FHC, ME). The fEPSPs were recorded in the current-clamp mode with ACSF-filled glass pipettes. Baseline responses were set at 30% of the maximum response. The test stimulus consisted of monophasic 0.1-ms pulses of constant current at 0.05 Hz. The paired-pulse ratio (PPR) was measured as the percentage change in fEPSP slope by giving paired pulses at 20, 50, 100, 150, and 200 ms intervals. The ratio was calculated as the second fEPSP slope value over the first slope value. LTP was induced by high-frequency stimulation (HFS: a train of 100 pulses in 1 s). The fEPSP slope values from 10-min baseline recording prior to HFS were normalized as 100%. Then fEPSPs evoked by HFS were recorded for 60 min. The slope values after HFS were formulated as percentage change from baseline. Two distinct phases were distinguished after HFS, short-term potentiation (STP) and LTP. The levels of STP and LTP were determined as the average of the percentage of slope values during the first 30 min and last 10 min after HFS, respectively. All recordings were made with a Multiclamp 700B amplifier and 1550B digitizer (Molecular Devices, Sunnyvale, CA) and analyzed with Clampfit 10.7 (Molecular Devices).

Behavioral Analysis

All behaviors were recorded by a video analysis system (Shanghai Jiliang Software Technology Co., Ltd., Shanghai, China). The investigators were blind to genotypes. Behavioral testing was performed between 09:00 and 18:00. All mice were habituated for 3 h in the behavioral room before starting the tests.

Open Field Test

Mice were placed in a chamber ($40 \times 40 \times 30$ cm^3) and their movements monitored. Beam-breaks were converted to directionally-specific movements and summed at 5-min intervals over a 30-min period. Ambulatory activity was measured as the total number of horizontal photobeam breaks (horizontal activity).

Elevated Plus Maze

A mouse was placed in the center of the elevated maze (50 cm above ground, with two open arms and one enclosed arm) and allowed to explore for 5 min. The number of entries into each arm and the time spent in the open arms were measured.

Light-Dark Box Test

The light-dark box had two equal-sized ($12 \times 30 \times 20$ cm^3) chambers, one light and one dark. A mouse was placed in the center of the light chamber and allowed to explore for 10 min. The times spent in the light and dark chambers were recorded.

Morris Water Maze (MWM)

Mice were trained for 5 days with 4 trials/day (2 min/trial, 30 min inter-trial intervals). We used 7 start positions to ensure that visuospatial memory was used to find the hidden platform. On the last day (day 5) at the end of the 3rd trial, a 60-s probe trial was run, in which the platform was removed and the mice were placed into the pool at a new start position and scored for the number of platform crossings. On day 6, mice were tested for the ability to find the visible platform within 60 s. If a mouse had 2 trials of 60 s, it was eliminated from the study.

Contextual Fear Conditioning

The fear conditioning experiments were performed according to the original protocol by Paylor *et al.* [23] with minor modifications. During the procedure an aversive, unconditioned stimulus (US, a foot shock), was paired with a conditioned stimulus (CS, the original testing chamber with 80 dB white noise) to elicit a freezing response. On the first day, the mice were placed in the testing chamber and allowed to acclimate for 5 min. On day 2, they were first allowed to explore the testing chamber for 2 min (pre-US score). After this exploration, the mice received a 28-s 80 dB white noise following three 2-s, 0.75-mA foot shocks, which served as the US. Again, the mice were allowed to explore for 2 min (post-US score). Twenty-four hours later the animals were returned to the testing chamber to explore for 5 min in the same context as the previous day (paired-test score). Ninety minutes later the animals were returned to the test chamber, but now the grid floor was hidden with a Plexiglas plate and sawdust to alter the context of the testing chamber. The animals were observed for 3 min (unpaired-test score).

Statistics

Data are presented as the mean ± SEM. Two-way ANOVA was used for behavioral analyses, including the open field test and MWM, and electrophysiological studies, including input-output (I/O) curve, PPR, and LTP. One-way ANOVA was used to analyze data from three or more groups. Student's *t*-test was used to compare data from two groups. A two-tailed P value < 0.05 was considered statistically significant. Comparisons were performed using SPSS (version 21.0) with appropriate inferential methods as indicated in the figure legends.

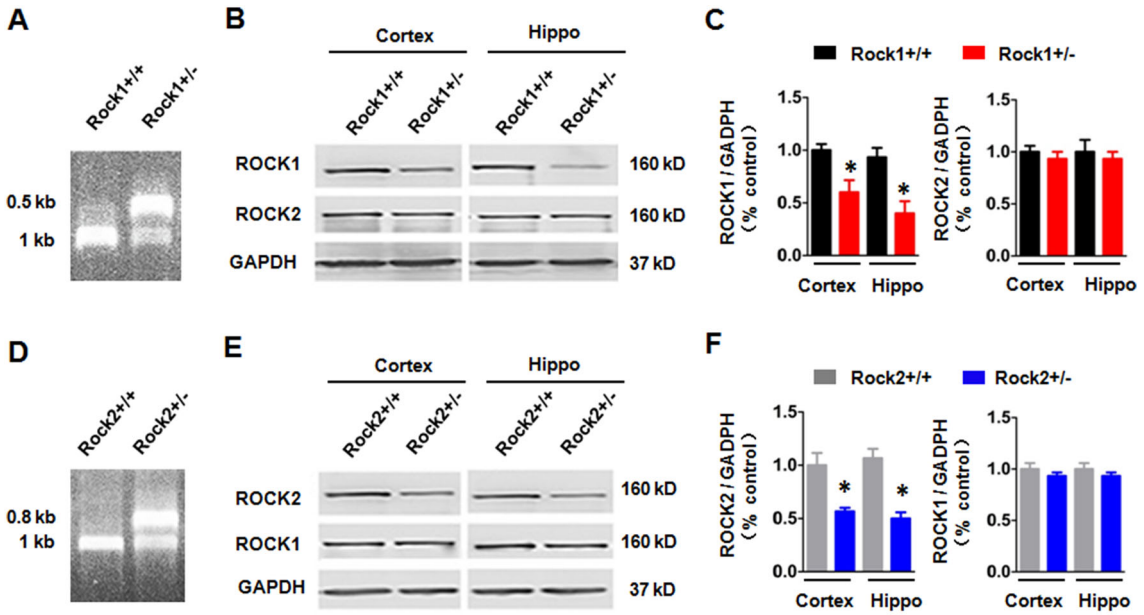

Fig. 1 No compensation for ROCK1 and 2 gene expression in Rock2$^{+/-}$ and Rock1$^{+/-}$ partial-knockout mice. **A** Genotyping by PCR analysis of genomic DNA from Rock1$^{+/+}$ and Rock1$^{+/-}$ mice. **B** ROCK1 and ROCK2 protein accumulation in the cortex and hippocampus (Hippo) of Rock1$^{+/-}$ mice and Rock1$^{+/+}$ control littermates. **C** Quantitative expression of the two ROCK isoforms in the cortex and hippocampus of Rock1$^{+/+}$ (black bars) and Rock1$^{+/-}$ (red bars) mice (n = 3 mice/group; cortex, $t(4) = 3.098$, $P < 0.05$; hippocampus, $t(4) = 3.671$, $P < 0.05$, *t*-test). **D** Genotyping by PCR analysis of genomic DNA from Rock2$^{+/+}$ and Rock2$^{+/-}$ mice. **E** Levels of ROCK1 and ROCK2 protein in the cortex and hippocampus of Rock2$^{+/-}$ mice and control littermates. **F** Quantitative expression of the two ROCK isoforms in the cortex and hippocampus of Rock2$^{+/+}$ (gray bars) and Rock2$^{+/-}$ (blue bars) mice (n = 3 mice/group; hippocampus, $t(4) = 3.606$, $P < 0.05$; cortex, $t(4) = 5.376$, $P < 0.05$). *$P < 0.05$ *versus* control group, *t*-test.

Results

Verification of Rock1 and Rock2 Heterozygous Mutant Mice

C57BL/6 mice are commonly used in studies of synaptic function and behavior. However, null mutations in Rock1 and Rock2 on the C57BL/6 background do not survive to adulthood [17]. Therefore, we used Rock1 and Rock2 heterozygous mutant mice (Fig. 1A, D). Both Rock1$^{+/-}$ and Rock2$^{+/-}$ mice had normal viability and body weight (data not shown) [20]. The levels of ROCK1 protein in the hippocampus and cerebral cortex were reduced by about half in Rock1$^{+/-}$ but not Rock2$^{+/-}$ mice (Fig. 1B, C). On the other hand, the levels of ROCK2 protein in the hippocampus and cerebral cortex were reduced by about half in Rock2$^{+/-}$ but not Rock1$^{+/-}$ mice (Fig. 1E, F). These results demonstrate the validity of using Rock1$^{+/-}$ and Rock2$^{+/-}$ mice to study the functions of these isoforms.

Abnormal Spine Density and Morphology in Rock1$^{+/-}$ and Rock2$^{+/-}$ Mice

Next, we investigated whether spine density and morphology are altered in Rock1$^{+/-}$ and Rock2$^{+/-}$ mice. Golgi staining was used to analyze the spines from the secondary and tertiary apical dendrites of CA1 pyramidal neurons. As shown in Fig. 2A–E, the spine density was reduced, but the spine morphology was normal in Rock1$^{+/-}$ mice. The spine density was also reduced in Rock2$^{+/-}$ mice, but the degree of reduction was greater than that in Rock1$^{+/-}$ mice

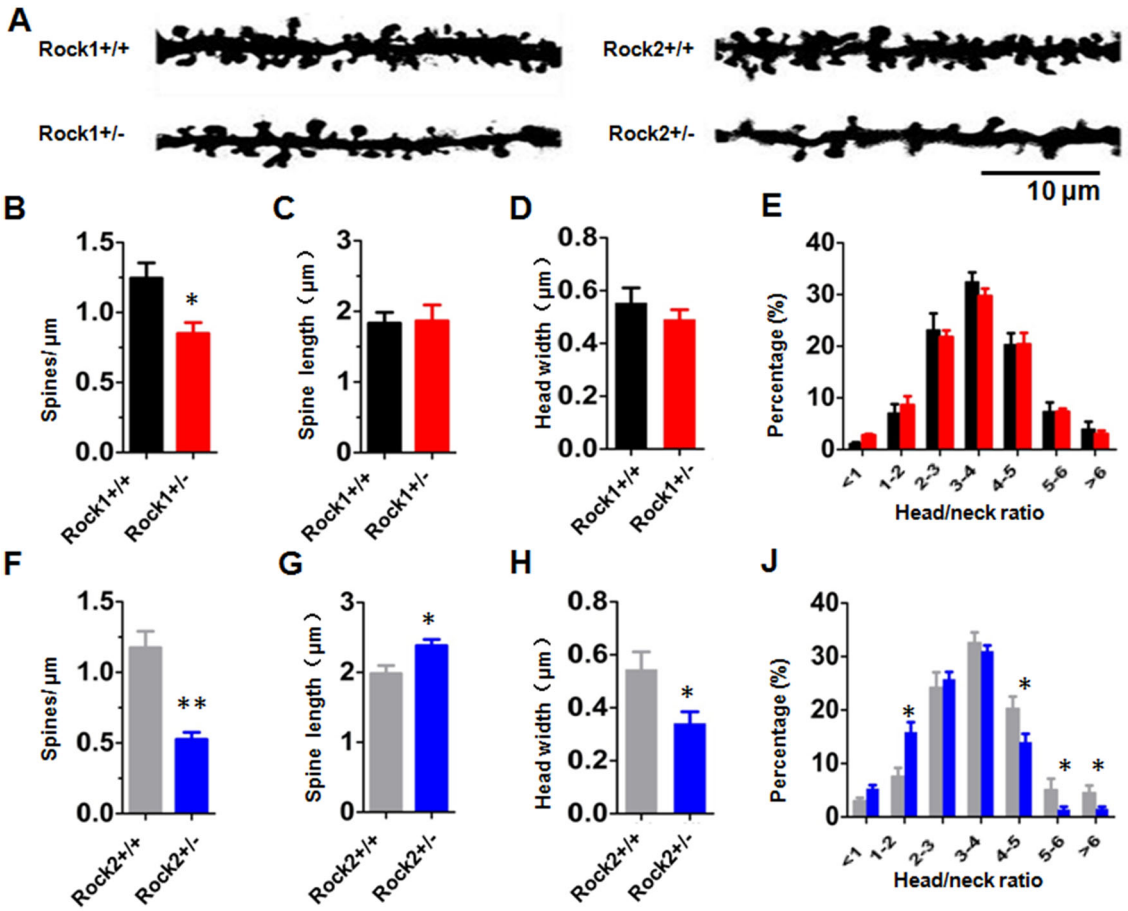

Fig. 2 Rock1$^{+/-}$ and Rock2$^{+/-}$ mice showed reduced spine density in hippocampal CA1 neurons. **A** Representative dendrites of Golgi-impregnated pyramidal neurons in the hippocampal CA1 stratum radiatum from Rock1$^{+/-}$ and Rock2$^{+/-}$ mice and their control littermates. **B–E** Quantitative data showing that spine density (**B**) in Rock1$^{+/-}$ mice (red bars) was lower than in Rock1$^{+/+}$ mice (black bars), but that spine length (**C**), head width (**D**), and head/neck ratio (**E**) were not affected (n = 9 segments from 3 mice/group; spine density, $t(22) = 2.950$, $P < 0.05$, t-test,; spine length, $t(22) = 0.545$, $P > 0.05$, t-test; spine head width, $t(118) = 0.938$, $P = 0.359$, t test). **F–J** Quantitative data showing reduced spine density (**F**) and spine width (**H**), increased spine length (**G**) and altered head/neck ratio (**J**) in Rock2$^{+/-}$ mice (blue bars) compared with Rock2$^{+/+}$ mice (gray bars) (n = 9 segments from 3 mice/group; spine density, $t(22) = 0.545$, $P < 0.05$, t-test; spine length, $t(22) = 2.780$, $P < 0.05$, t-test; spine head width, $t(118) = 2.612$; $P = 0.016$, t test). $^*P < 0.05$, $^{**}P < 0.01$.

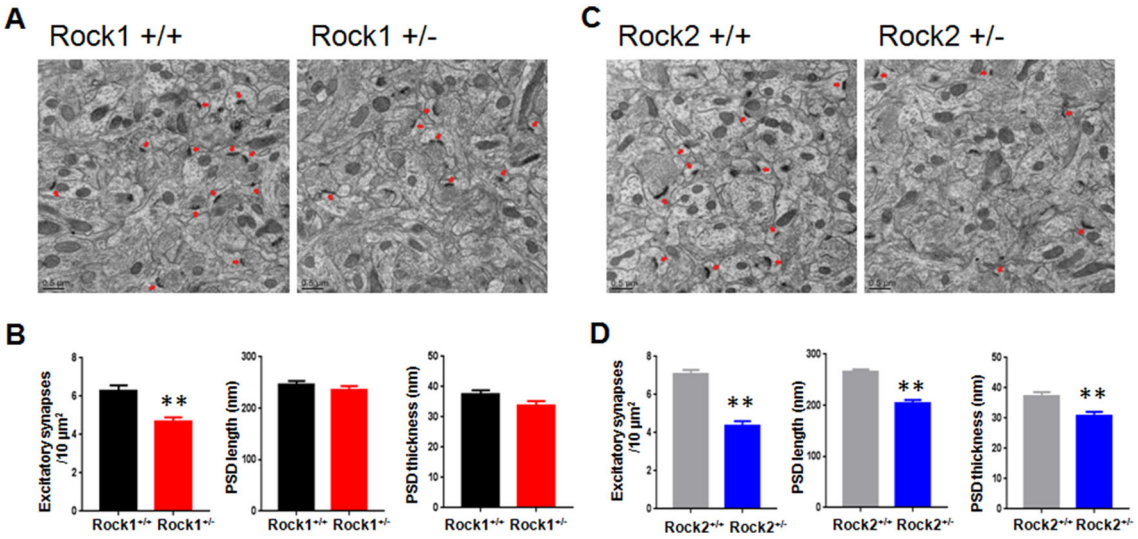

Fig. 3 Rock1$^{+/-}$ and Rock2$^{+/-}$ mice had fewer excitatory synapses in hippocampal CA1. **A** Representative EM images in the CA1 region of control and Rock1$^{+/-}$ mice. **B** Comparable numbers of excitatory synapses and PSD length and thickness in the CA1 region of Rock1$^{+/-}$ mice and their control littermates (n = 90 images from 3 mice/group; excitatory synaptic density, P = 0.0002, two-tailed Mann-Whitney test; PSD length, t = 1.091, P = 0.2691, unpaired t-test; PSD thickness, t = 1.844, P = 0.0668, unpaired t-test). **C** Representative EM images in the CA1 region of control and Rock2$^{+/-}$ mice. **D** Comparable numbers of excitatory synapses and PSD length and thickness in the CA1 region in Rock2$^{+/-}$ and their control littermates (n = 90 images from 3 mice/group; excitatory synaptic density, t = 8.509, $P < 0.0001$, unpaired t test; PSD length, $P < 0.0001$, two-tailed Mann-Whitney test; PSD thickness, t = 3.529, $P < 0.0005$, unpaired t-test). $^{**}P < 0.01$.

(Fig. 2A, B, F). Strikingly, the spine morphology also changed, as evidenced by the increased spine length and decreased spine width in Rock2$^{+/-}$ mice (Fig. 2A, G, H). Accordingly, the spine head/neck ratio was altered in Rock2$^{+/-}$ but not Rock1$^{+/-}$ mice (Fig. 2E, J). Taken together, these results suggest that ROCK1 only regulates spine density while ROCK2 is crucial for regulating both the density and morphology of spines in CA1 hippocampal neurons.

Reduced Excitatory Synapse Density in Rock1$^{+/-}$ and Rock2$^{+/-}$ Mice

The majority of excitatory synapses in the rodent brain are located on dendritic spines. To further investigate whether the spine deficits in Rock1$^{+/-}$ and Rock2$^{+/-}$ mice reflect reduced numbers of synapses, we used transmission electron microscopy (EM) in the hippocampal CA1 region. We found fewer excitatory synapses in this region in both Rock1$^{+/-}$ and Rock2$^{+/-}$ mice than in their control littermates (Fig. 3A, C), in agreement with the Golgi staining. In addition, the Rock2$^{+/-}$ mice showed reduced PSD length and thickness compared with their control littermates (Fig. 3C, D), while the Rock1$^{+/-}$ mice appeared normal (Fig. 3A, B). Taken together, these results indicated decreased excitatory synaptic density in both Rock1$^{+/-}$ and Rock2$^{+/-}$ mice, and partial deletion of ROCK2 isoform alters the structure of excitatory synapses in the hippocampal CA1 region.

Compromised Glutamatergic Transmission in Rock1$^{+/-}$ and Rock2$^{+/-}$ Mice

To determine whether partial deletion of ROCK isoform affects excitatory synaptic transmission, we first measured the frequency and amplitude of mEPSCs in CA1 pyramidal neurons. We found that the frequency but not the amplitude of mEPSCs was reduced in Rock1$^{+/-}$ mice compared with that in Rock1$^{+/+}$ mice (Fig. 4A–C). By contrast, both the frequency and amplitude of mEPSCs were decreased in Rock2$^{+/-}$ mice (Fig. 4A, D, E). These results demonstrated that mutation of Rock2 has a more dramatic effect on synaptic function than mutation of Rock1, consistent with the morphological observations. To further assess the effects of ROCK1 and ROCK2 on basal glutamatergic transmission, we recorded fEPSPs at the Schaffer collateral (SC)–CA1 synapses. As shown in Fig. 5A and C, the I/O curves shifted downward in both Rock1$^{+/-}$ and Rock2$^{+/-}$ mice compared with those of the controls, suggesting impairment of glutamatergic transmission. The reduction in glutamatergic transmission in Rock1$^{+/-}$ and Rock2$^{+/-}$ mice is apparently not due to the alteration of presynaptic release because the PPRs of the fEPSPs was normal in both strains of mice (Fig. 5B, D).

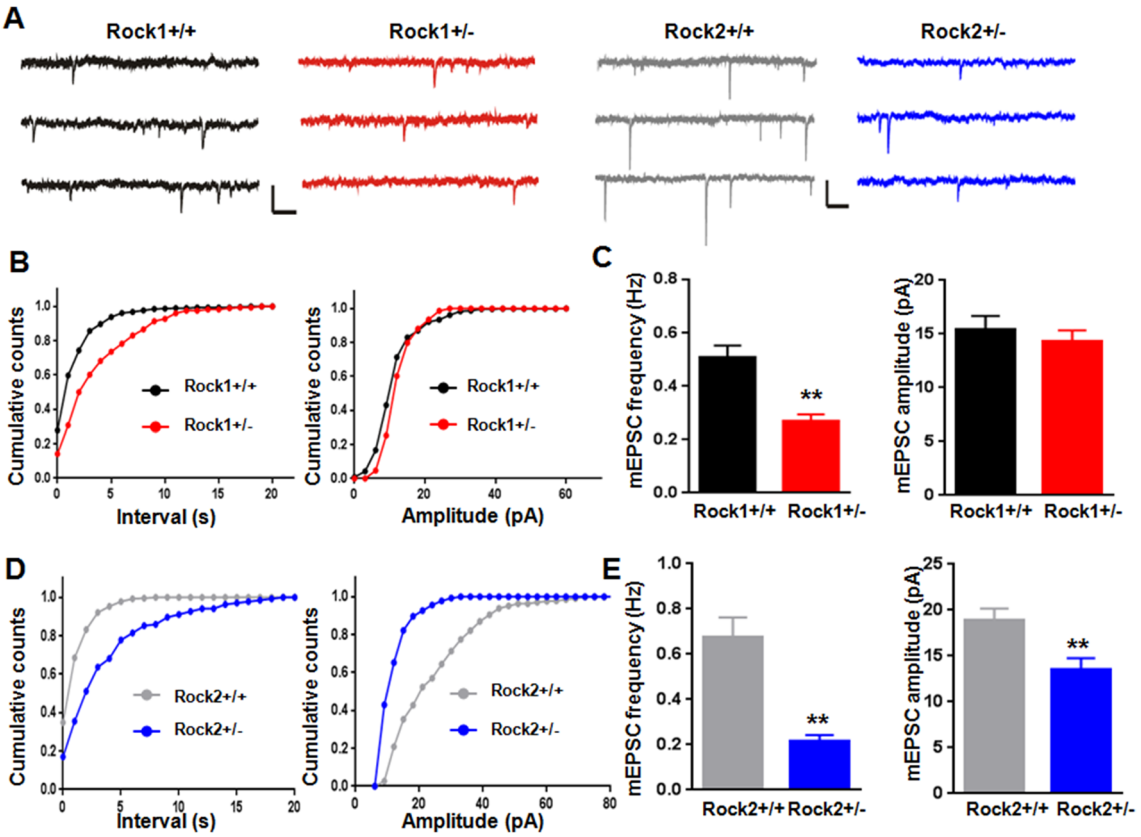

Fig. 4 Rock1$^{+/-}$ and Rock2$^{+/-}$ mice showed decreased synaptic function in hippocampal CA1. **A** Representative mEPSC traces. Black, Rock1$^{+/+}$; red, Rock1$^{+/-}$; grey, Rock2$^{+/+}$; blue, Rock2$^{+/-}$. Horizontal bar, 200 ms; vertical bar, 20 pA. **B** Cumulative distributions of mEPSC amplitudes (left) and intervals (right) in Rock1$^{+/-}$ (red) and Rock1$^{+/+}$ (black) control neurons. **C** The frequencies (left), but not amplitudes (right), of mEPSCs in Rock1$^{+/-}$ mice (red bars), are reduced compared with those of their Rock1$^{+/+}$ (black bars) littermates (n = 12 cells from 3 mice (both genotypes); t = 4.674, $P <$ 0.0001 for frequency; t = 0.6223, P = 0.5401 for amplitude; unpaired t-test. **D** Cumulative distributions of mEPSC amplitudes (left) and intervals (right) in Rock2$^{+/-}$ (blue) and Rock2$^{+/+}$ control (gray) neurons. **E** The frequencies (left) and amplitudes (right) of mEPSCs were lower in Rock2$^{+/-}$ mice (blue bars) than in Rock2$^{+/+}$ control mice (gray bars) (n = 12 cells from 3 mice (both genotypes); t = 3.882, P = 0.0008 for frequency; t = 5.009, $P <$ 0.0001 for amplitude; unpaired t-test). $^{**}P < 0.01$.

To study the modulation of synaptic plasticity by ROCK, we determined the levels of STP and LTP at SC–CA1 synapses using an HFS protocol [24–26]. The slope of fEPSPs in the first 30 min (STP) after HFS was normal in Rock1$^{+/-}$ preparations, but LTP was significantly attenuated in Rock1$^{+/-}$ mice relative to Rock1$^{+/+}$ mice (Fig. 5E, F). In striking contrast, HFS did not induce the characteristic STP-LTP sequence in Rock2$^{+/-}$ hippocampal slices; both STP and LTP were impaired in Rock2$^{+/-}$ mice relative to Rock2$^{+/+}$ mice (Fig. 5G and H). These data indicate that the activities of both ROCK1 and 2 are essential for the generation of LTP induced by high-frequency electrical stimulation at the SC-CA1 synapse, and ROCK2, but not ROCK1, is required for STP in hippocampal slices (Fig. 5G, H).

Impaired Hippocampus-Dependent Learning and Memory in Rock1$^{+/-}$ and Rock2$^{+/-}$ Mice

The above data demonstrated deficits of synapse formation and plasticity in the hippocampus of Rock1$^{+/-}$ and Rock2$^{+/-}$ mice. We next investigated whether hippocampus-dependent learning and memory tasks are also compromised. First, we used the MWM test to evaluate hippocampus-dependent spatial learning and memory in control and Rock-mutant mice. Both Rock1$^{+/-}$ and Rock2$^{+/-}$ mice had no visualization problems as they were able to locate the visible platform in the MWM (Fig. 6B, F). However, the escape latency to find the submerged platform was higher in both Rock mutants than in controls (Fig. 6A, C, G), indicating a compromised ability to learn. The increased escape latency was not likely due to defective motility since their locomotion in the open field was comparable to controls (Fig. S1). In the probe trial, the number of passes across the platform location and

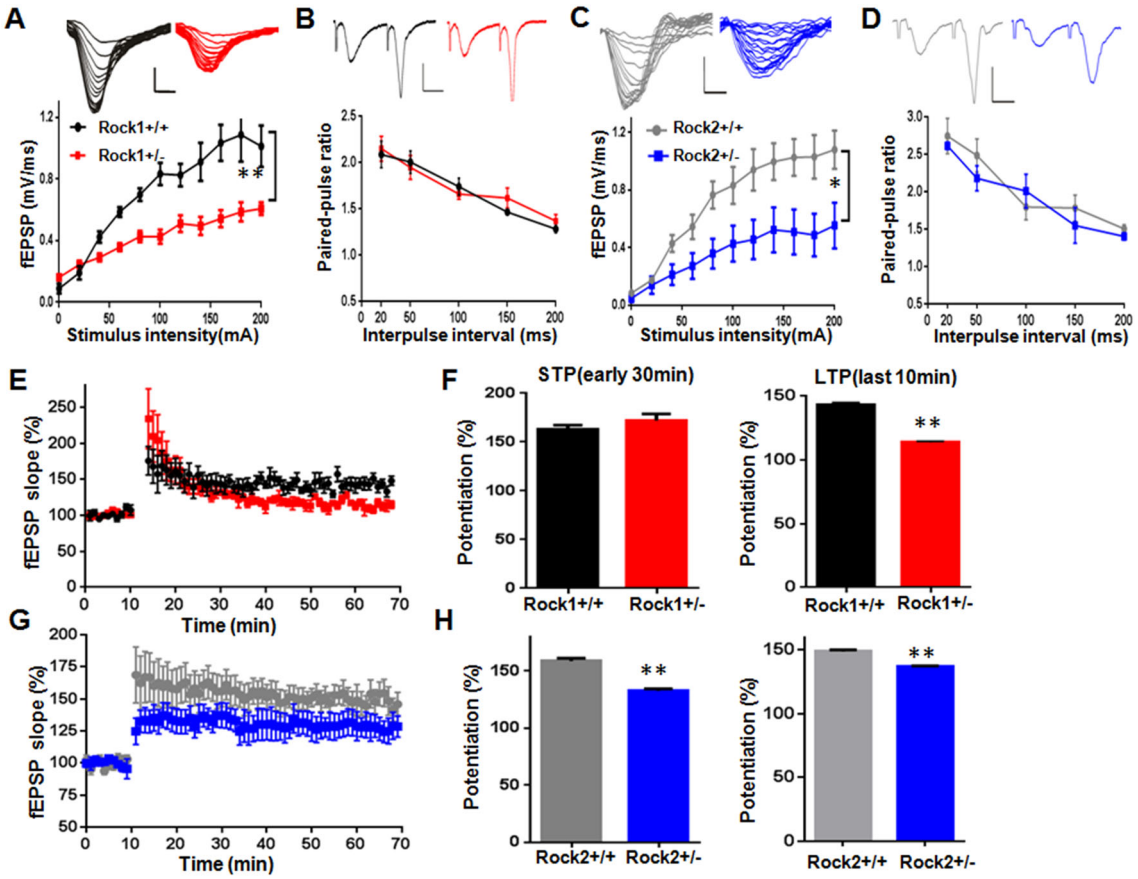

Fig. 5 Rock1$^{+/-}$ and Rock2$^{+/-}$ mice showed decreased synaptic plasticity in hippocampal CA1. **A** The I/O curves for Rock1$^{+/-}$ mice (red) are depressed compared with those of their Rock1$^{+/+}$ littermates (black). Upper panel, representative traces; lower panel, quantitative data (7 slices from 3 Rock1$^{+/-}$ mice and 9 slices from 3 control mice; group F = 17.820, P = 0.001, repeated measures two-way ANOVA). **B** The paired-pulse ratios of Rock1$^{+/-}$ (red) and control mice (black) did not differ (12 slices from 3 Rock1$^{+/-}$ mice and 11 slices from 3 control mice; genotype $F(1,105)$ = 0.2626, P = 0.6094, two-way ANOVA). **C** The I/O curves for Rock2$^{+/-}$ mice (blue) are depressed compared with those of their Rock2$^{+/+}$ control littermates (gray). Upper, representative traces; lower, quantitative data (8 slices from 3 Rock2$^{+/-}$ mice and 7 slices from 3 control mice; group F = 4.110, P = 0.064, repeated measures two-way ANOVA). (D) The paired-pulse ratios of Rock2$^{+/-}$ (blue) and control (gray) mice did not differ (6 slices from 3 Rock2$^{+/-}$ mice and 6 slices from 3 control mice; genotype $F(1,50)$ = 1.299, P = 0.2599, two-way ANOVA). **E** Normalized fEPSP slopes showing decreased LTP in Rock1$^{+/-}$ mice (red) compared with their littermate control (black). **F** Left, STP, quantitative analysis of data from the first 30 min; right, LTP, quantitative analysis of data from the last 30 min in Rock1$^{+/-}$ (red) and Rock1$^{+/+}$ (black) mice (6 slices from 3 Rock1$^{+/-}$ mice and 6 slices from 3 control mice; STP, t = 1017, P = 0.24, t-test; LTP, t = 15.93, $P < 0.0001$). **G** Rock2$^{+/-}$ mice (blue) had decreased LTP compared with their littermate control (gray). **H** Left, STP, quantitative analysis of data from the first 30 min; right, LTP, quantitative analysis of data from the last 30 min in Rock2$^{+/-}$ (blue) and Rock2$^{+/+}$ (gray) mice (6 slices from 3 Rock2$^{+/-}$ mice and 8 slices from 3 control mice; STP, t = 8.534, $P < 0.0001$; LTP, t = 13.09, $P < 0.0001$, t-test). *$P < 0.05$; **$P < 0.01$.

the time in the target quadrant was lower in both Rock1$^{+/-}$ and Rock2$^{+/-}$ mice than in controls (Fig. 6D, E, H, I). These results indicated that spatial reference memory is impaired in both Rock1$^{+/-}$ and Rock2$^{+/-}$ mice.

Next, we determined whether the downregulation of ROCK1 or 2 affects contextual fear memory, which is also hippocampus-dependent. The freezing time before and immediately after the foot shock was indistinguishable between Rock mutant mice and controls (Fig. 7A). The Rock1$^{+/-}$ and Rock2$^{+/-}$ mice also behaved normally during the unpaired test (Fig. 7C, D). However, the freezing time during the paired test was significantly lower for the Rock mutant mice than the controls (Fig. 7C and D), suggesting that contextual fear learning is impaired in the mutant mice. By contrast, the Rock mutant mice did not show anxiety-like behavior in the elevated plus-maze and light-dark box (Fig. S2A, B, D, E) or a depression-like phenotype in the forced swimming test (Fig. S2C, F).

Discussion

We performed a comparative study of the function of ROCK1 and ROCK2 in hippocampal spine formation and synaptic function and have presented data at the molecular (ROCK

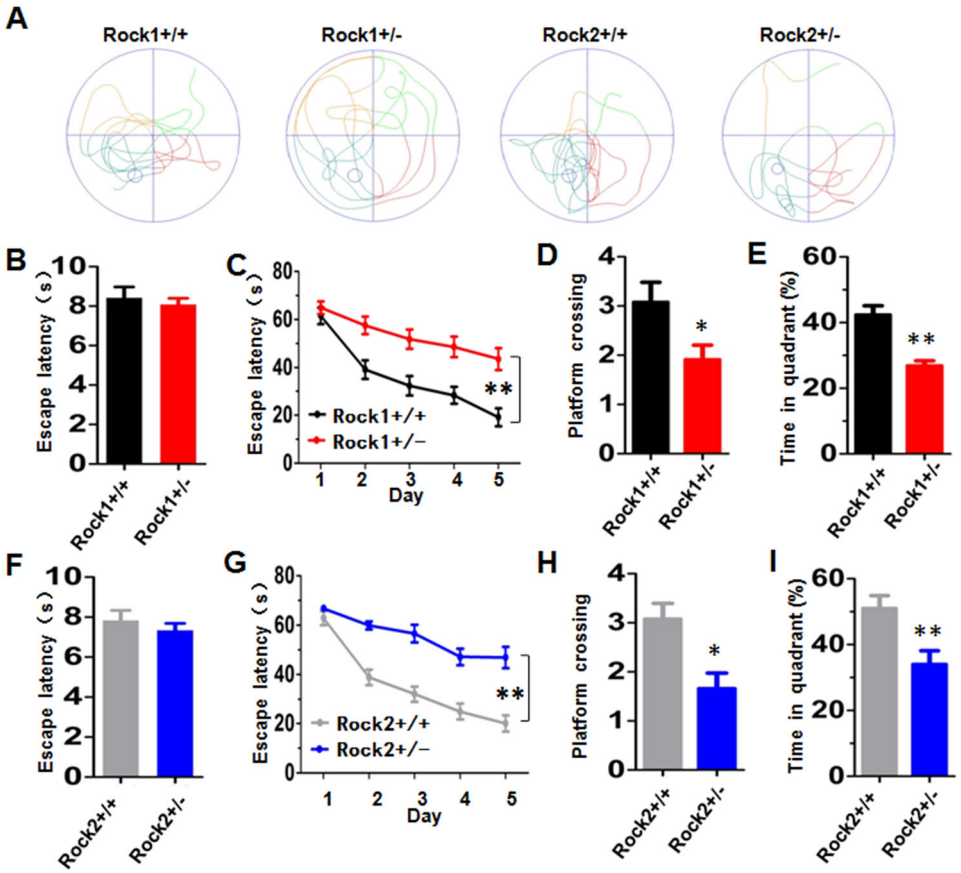

Fig. 6 Impaired spatial learning and memory in both Rock1$^{+/-}$ and Rock2$^{+/-}$ mice. **A** Representative images showing the swim paths of mice during the water maze test. **B** Quantitative data showing that the escape latency, or the time it took for mice to swim to the visible platform in the water maze, did not differ between Rock1$^{+/-}$ mice (red) and their Rock1$^{+/+}$ littermates (black) ($t(22) = 0.522$, $P = 0.607$). **C** Quantitative data showing that the escape latency for the hidden platform in the water maze was longer for Rock1$^{+/-}$ mice (red) than for their control littermates (black) ($F(1,22) = 17.117$, $P < 0.001$, two-way ANOVA). **D**, **E** Quantitative data showing reduced number of platform crossings and time in the right quadrant for Rock1$^{+/-}$ mice (red) compared with their control littermates (black) ($n = 12$ mice for both groups; platform crossing, $t(22) = 2.376$, $P = 0.027$; time in quadrant, $t(22) = 4.736$, $P < 0.001$). **F** Quantitative data showing that the escape latency for Rock2$^{+/-}$ mice (blue), or the time it took to swim to the visible platform, did not differ from that of their control littermates (gray) ($t(22) = 0.810$, $P = 0.427$, *t*-test). **G** Quantitative data showing increased escape latency for the hidden platform was higher for Rock2$^{+/-}$ mice (blue) than for their control littermates (gray) ($F(1,22) = 33.025$, $P < 0.001$, two-way ANOVA). **H**, **I** Quantitative data showing a reduced number of platform crossings and time in the right quadrant for Rock2$^{+/-}$ mice compared with their control littermates ($n = 12$ mice for both groups; platform crossing, $t(22) = 3.143$, $P = 0.005$; time in quadrant, $t(22) = 3.228$, $P = 0.004$). $^{*}P < 0.05$; $^{**}P < 0.01$ *versus* control group, *t*-test.

expression levels), cellular (spine structure), circuit (synaptic transmission), and cognitive (behavior) levels. Our major findings are as follows. First, heterozygotic Rock-mutant mice specifically decreased the expression levels of either ROCK1 or ROCK2, without affecting the other. Second, spine density was reduced in both Rock1$^{+/-}$ and Rock2$^{+/-}$ mice. However, excitatory synapses structure was only altered in Rock2$^{+/-}$ mice. Third, the mEPSC frequency was reduced in both Rock1$^{+/-}$ and Rock2$^{+/-}$ mice, but only Rock2$^{+/-}$ mice showed decreased mEPSC amplitude. Both Rock1$^{+/-}$ and Rock2$^{+/-}$ mice had impaired LTP induction, but only ROCK2 was essential for the generation of STP. Finally, hippocampus-dependent learning and memory was compromised in both Rock1$^{+/-}$ and Rock2$^{+/-}$ mice.

Although ROCKs have been implicated in spine formation and synaptic function [27, 28], our study, for the first time, addressed the distinctive roles of ROCK isoforms in hippocampal synapse formation and function *in vivo*. Our data suggest that ROCK2 is more critical for spine formation and synaptic function than ROCK1. These distinct roles of ROCK1 and ROCK2 may be due to their different subcellular distributions or to their action on different substrates. For example, Newell-Litwa *et al.* showed that ROCK1 and ROCK2 are strongly expressed in actomyosin filament bundles along the cell periphery, but ROCK2 is additionally localized to actin filaments within protrusions [29]. Shi *et al.* demonstrated that ROCK1

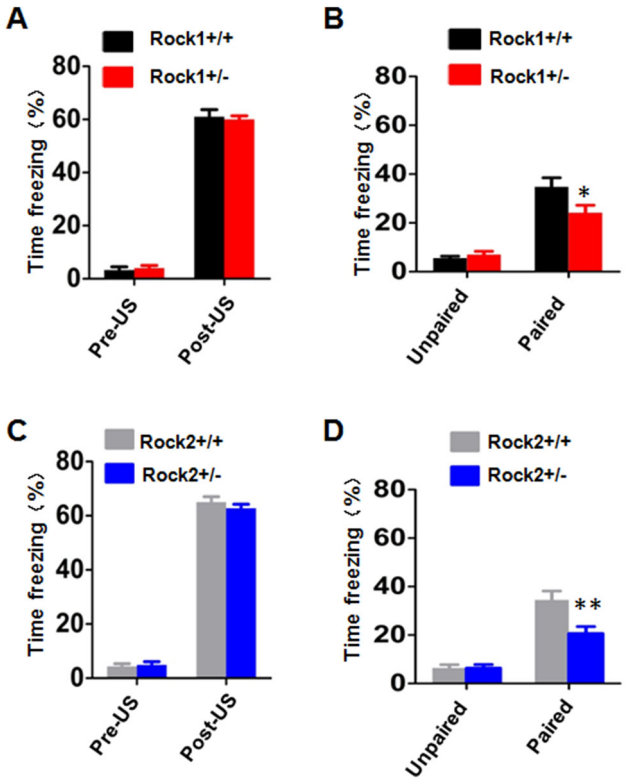

Fig. 7 Rock1$^{+/-}$ and Rock2$^{+/-}$ mice exhibited deficits in fear conditioning. **A**, **C** Quantitative data showing that both Rock1$^{+/-}$ (red) and Rock2$^{+/-}$ mice (blue) had freezing times similar to their Rock1$^{+/+}$ (black) and Rock2$^{+/+}$ (gray) control littermates under pre-US and post-US conditions (Rock1, pre-US, $t(22) = 0.3804$, $P = 0.7073$; post-US, $t(22) = 1.615$, $P = 0.1206$; Rock2, pre-US, $t(22) = 0.7541$, $P = 0.4588$; post-US, $t(22) = 1.318$, $P = 0.2011$, unpaired t test). **B**, **D** Contextual conditioning. Quantitative data showing that both Rock1$^{+/-}$ (red) and Rock2$^{+/-}$ (blue) mice had a significantly longer freezing time after 24 h of training than their Rock1$^{+/+}$ (black) and Rock2$^{+/+}$ (gray) control littermates (n = 12 mice/group; Rock1, unpaired test, $t(22) = 0.054$, $P = 0.818$; paired test, $t(22) = 4.804$, $P = 0.039$; Rock2, unpaired test, $t(22) = 0.005$, $P = 0.946$; paired test, $t(22) = 8.870$, $P = 0.007$; unpaired t-test). $^{*}P < 0.05$; $^{**}P < 0.001$.

destabilizes actin through MLC phosphorylation, whereas ROCK2 stabilizes actin *via* cofilin phosphorylation [16].

One previous study reported that spine density is normal on the basis of analyzing MAP2-positive processes in cultured Rock2-knockout (Rock2$^{-/-}$) hippocampal neurons [10]. However, in Rock2$^{+/-}$ mice, the spine density in the hippocampal CA1 region was lower than in control mice in our study using Golgi staining in hippocampal sections (Fig. 2). Meanwhile, Zhou *et al.* reported that many of the Rock2-knockout spines appear to be filopodium-like structures in cultured neurons [10], but we found no filopodium-like structures in the CA1 region (Fig. 2). We noted that the differences between the two studies included mice on different genetic backgrounds (CD1 *versus* C57/BL), experimental models (*in vitro versus in vivo*), and genetic mutations (homozygous *versus* heterozygous). One interpretation of the different synaptic phenotypes might be the different adaptive or compensatory mechanisms between homozygotes and heterozygotes. For example, a previous study showed differences between heterozygous and homozygous Shank3-deficient mice, including more perforated synapses in the heterozygous than in the homozygous mice [30].

Consistent with the notion that the frequency of mEPSC recorded at the soma is positively correlated with the density of dendritic spines [31, 32], the reduction in the frequency of mEPSCs in both Rock1$^{+/-}$ and Rock2$^{+/-}$ mice is consistent with the reduced spine density revealed by Golgi staining and EM studies. Interestingly, Golgi staining showed increased spine length in Rock2$^{+/-}$ but not Rock1$^{+/-}$ mice. Moreover, we found a reduction in PSD length and thickness from EM images in Rock2$^{+/-}$ but not in Rock1$^{+/-}$ mice (Fig. 4). All these results indicated that ROCK2 but not ROCK1 is important for the spine morphology and PSD area of synapses. It has been reported that longer spines produce smaller EPSCs than shorter ones [31, 33, 34], and the efficacy of synaptic transmission is strongly correlated with spine length, spine head width, and PSD area [31, 35, 36]. Thus, in accord with the structural changes, Rock2$^{+/-}$ mice showed more severe deficits in mEPSC frequency and amplitude than Rock1$^{+/-}$ mice.

Furthermore, LTP was significantly impaired in both ROCK isoform partial knockout mice compared with their control littermates. These findings support the notion that both ROCK isoforms contribute to hippocampal synaptic plasticity, consistent with previous studies in which hippocampal slices were treated with a ROCK inhibitor [37, 38]. Our study is the first to identify the critical role of ROCK1 and ROCK2 in LTP induction. In addition, although both the PPRs of fEPSPs and STP are associated with presynaptic modulation, PPR correlates better with changes in the number of transmitter quanta released from the presynaptic terminal after basic and repeated stimulation [39, 40]. So, the preservation of PPRs in both Rock1$^{+/-}$ and Rock2$^{+/-}$ mice indicates that the number of presynaptic vesicles and fractional release is normal. However, STP is not only associated with increased fractional release, but also to an increased size of the releasable pool of vesicles and to Ca^{2+} uptake and release by mitochondria [41, 42]. As shown in Figure 5F and 5H, Rock2$^{+/-}$ mice showed deficits in STP while Rock1$^{+/-}$ mice did not, suggesting that there were aberrant presynaptic changes in Rock2$^{+/-}$ but not in Rock1$^{+/-}$ mice. Thus, taken together, these results support the idea that both ROCK isoforms are involved in excitatory postsynaptic transmission and synaptic plasticity, but the ROCK2 isoform is involved in both presynaptic and postsynaptic

changes while the ROCK1 isoform is only involved in postsynaptic changes.

ROCKs are widely expressed in several brain regions including the prefrontal cortex, hippocampus, and dorsal striatum [43, 44]. In this study, we focused on the functions of ROCK isoforms in the hippocampus. It remains to be determined whether ROCK1 and ROCK2 play similar roles in spine formation and synaptic function in other brain regions. We used haplo-insufficient mutants to study the physiological roles of ROCK isoforms in synapse formation and function. However, the ROCK signaling pathway is abnormally activated in some brain disorders. For example, LIM kinase 1 (LIMK1), an important substrate of ROCKs in the regulation of actin dynamics, is duplicated in some patients with autism and schizophrenia [45, 46]. Recent studies have also implicated the activation of LIMK1-cofilin in mouse genetic models of schizophrenia [21]. Accordingly, ROCKs are attractive drug targets for a range of brain disorders [28, 38, 47]. However, a critical question in ROCK-based treatment is whether ROCKs play isoform-specific roles in neuronal structure and function. Our study provides evidence that ROCKs do in fact have isoform-specific roles.

Acknowledgements We thank Dr. R William Caldwell (Department of Pharmacology and Toxicology, Medical College of Georgia, Augusta, GA, 30912-2300, USA) for providing the transgenic Rock1$^{+/-}$ and Rock2$^{+/-}$ mice. This work was supported by the National Science Foundation of China (81774406 and 31571041), the Guangdong Innovative and Entrepreneurial Research Team Program (Natural Science) (2017KCXTD006), Guangdong Province Universities and Colleges Pearl River Scholar Funded Scheme (2016), and the Scientific Research and Innovation Team Program of Guangzhou University of Chinese Medicine (2017KYTD03).

Compliance with Ethical Standards

Conflict of interest The authors declare that they have no competing interests.

References:

1. Bellot A, Guivernau B, Tajes M, Bosch-Morató M, Valls-Comamala V, Muñoz FJ. The structure and function of actin cytoskeleton in mature glutamatergic dendritic spines. Brain Res 2014, 1573: 1–16.
2. Bacon C, Endris V and Rappold GA. The cellular function of srGAP3 and its role in neuronal morphogenesis. Mech Dev 2013, 130: 391–395.
3. Tomasoni R, Repetto D, Morini R, Elia C, Gardoni F, Di Luca M, *et al.* SNAP-25 regulates spine formation through postsynaptic binding to p140Cap. Nat Commun 2013, 4: 2136.
4. Amano M, Tsumura Y, Taki K, Harada H, Mori K, Nishioka T, *et al.* A proteomic approach for comprehensively screening substrates of protein kinases such as Rho-kinase. PLoS One 2010, 5: e8704.
5. Fukata M, Nakagawa M, Kaibuchi K. Roles of Rho-family GTPases in cell polarisation and directional migration. Curr Opin Cell Biol 2003, 15: 590–597.
6. Etienne-Manneville S, Hall A. Rho GTPases in cell biology. Nature 2002, 420: 629–635.
7. Hall A. Rho GTPases and the actin cytoskeleton. Science 1998, 279: 509–514.
8. Matsui T, Amano M, Yamamoto T, Chihara K, Nakafuku M, Ito M, *et al.* Rho-associated kinase, a novel serine/threonine kinase, as a putative target for small GTP binding protein Rho. EMBO J 1996, 15: 2208–2216.
9. Swanger SA, Mattheyses AL, Gentry EG, Herskowitz JH. ROCK1 and ROCK2 inhibition alters dendritic spine morphology in hippocampal neurons. Cell Logist 2015, 5: e1133266.
10. Zhou Z, Meng Y, Asrar S, Todorovski Z, Jia Z. A critical role of Rho-kinase ROCK2 in the regulation of spine and synaptic function. Neuropharmacology 2009, 56: 81–89.
11. Schmandke A, Schmandke A, Strittmatter SM. ROCK and Rho: Biochemistry and neuronal functions of Rho-associated protein kinases. Neuroscientist 2007, 13: 454–469.
12. Amano M, Nakayama M, Kaibuchi K. Rho-kinase/ROCK: A key regulator of the cytoskeleton and cell polarity. Cytoskeleton (Hoboken) 2010, 67: 545–554.
13. Amano M, Ito M, Kimura K, Fukata Y, Chihara K, Nakano T, *et al.* Phosphorylation and activation of myosin by Rho-associated kinase (Rho-kinase). J Biol Chem 1996, 271: 20246–20249.
14. Kimura K, Eguchi S. Angiotensin II type-1 receptor regulates RhoA and Rho-kinase/ROCK activation via multiple mechanisms. Focus on "Angiotensin II induces RhoA activation through SHP2-dependent dephosphorylation of the RhoGAP p190A in vascular smooth muscle cells". Am J Physiol Cell Physiol 2009, 297: C1059–C1061.
15. Sumi T, Matsumoto K and Nakamura T. Specific activation of LIM kinase 2 via phosphorylation of threonine 505 by ROCK, a Rho-dependent protein kinase. J Biol Chem 2001, 276: 670–676.
16. Shi J, Wu X, Surma M, Vemula S, Zhang L, Yang Y, *et al.* Distinct roles for ROCK1 and ROCK2 in the regulation of cell detachment. Cell Death Dis 2013, 4: e483.
17. Thumkeo D, Keel J, Ishizaki T, Hirose M, Nonomura K, Oshima H, *et al.* Targeted disruption of the mouse rho-associated kinase 2 gene results in intrauterine growth retardation and fetal death. Mol Cell Biol 2003, 23: 5043–5055.
18. Shimizu Y, Thumkeo D, Keel J, Ishizaki T, Oshima H, Oshima M, *et al.* ROCK-I regulates closure of the eyelids and ventral body wall by inducing assembly of actomyosin bundles. J Cell Biol 2005, 168: 941–953.
19. Zhang Z, Ottens AK, Larner SF, Kobeissy FH, Williams ML, Hayes RL, *et al.* Direct Rho-associated kinase inhibition [correction of inhibiton] induces cofilin dephosphorylation and neurite outgrowth in PC-12 cells. Cell Mol Biol Lett 2006, 11: 12–29.
20. Yao L, Chandra S, Toque HA, Bhatta A, Rojas M, Caldwell RB, *et al.* Prevention of diabetes-induced arginase activation and vascular dysfunction by Rho kinase (ROCK) knockout. Cardiovasc Res 2013, 97: 509–519.
21. Yin DM, Chen YJ, Lu YS, Bean JC, Sathyamurthy A, Shen C, *et al.* Reversal of behavioral deficits and synaptic dysfunction in mice overexpressing neuregulin 1. Neuron 2013, 78: 644–657.
22. Gibb R, Kolb B. A method for vibratome sectioning of Golgi-Cox stained whole rat brain. J Neurosci Methods 1998, 79: 1-4.
23. Paylor R, Tracy R, Wehner J, Rudy JW. DBA/2 and C57BL/6 mice differ in contextual fear but not auditory fear conditioning. Behav Neurosci 1994, 108: 810–817.
24. Chan CB, Chen Y, Liu X, Tang X, Lee CW, Mei L, *et al.* PIKE-mediated PI3-kinase activity is required for AMPA receptor surface expression. EMBO J 2011, 30: 4274–4286.

25. Kamal A, Ramakers GM, Altinbilek B, Kas MJ. Social isolation stress reduces hippocampal long-term potentiation: Effect of animal strain and involvement of glucocorticoid receptors. Neuroscience 2014, 256: 262–270.
26. Chen Y, Behnisch T. The role of gamma-secretase in hippocampal synaptic transmission and activity-dependent synaptic plasticity. Neurosci Lett 2013, 554: 16–21.
27. Bobo-Jiménez V, Delgado-Esteban M, Angibaud J, Sánchez-Morán I, de la Fuente A, Yajeya J, *et al.* APC/C(Cdh1)-Rock2 pathway controls dendritic integrity and memory. Proc Natl Acad Sci U S A 2017, 114: 4513–4518.
28. García-Rojo G, Fresno C, Vilches N, Díaz-Véliz G, Mora S, Aguayo F, *et al.* The ROCK inhibitor fasudil prevents chronic restraint stress-induced depressive-like behaviors and dendritic spine loss in rat hippocampus. Int J Neuropsychopharmacol 2017, 20: 336–345.
29. Newell-Litwa KA, Badoual M, Asmussen H, Patel H, Whitmore L, Horwitz AR. ROCK1 and 2 differentially regulate actomyosin organization to drive cell and synaptic polarity. J Cell Biol 2015, 210: 225–242.
30. Uppal N, Puri R, Yuk F, Janssen WG, Bozdagi-Gunal O, Harony-Nicolas H, *et al.* Ultrastructural analyses in the hippocampus CA1 field in Shank3-deficient mice. Mol Autism 2015, 6: 41.
31. Segal M. Dendritic spines, synaptic plasticity and neuronal survival: Activity shapes dendritic spines to enhance neuronal viability. Eur J Neurosci 2010, 31: 2178–2184.
32. Yin DM, Chen YJ, Liu S, Jiao H, Shen C, Sathyamurthy A, *et al.* Calcyon stimulates neuregulin 1 maturation and signaling. Mol Psychiatry 2015, 20: 1251–1260.
33. Zito K. The flip side of synapse elimination. Neuron 2003, 37: 1–2.
34. Araya R, Jiang J, Eisenthal KB, Yuste R. The spine neck filters membrane potentials. Proc Natl Acad Sci U S A 2006, 103: 17961–17966.
35. Yin DM, Sun XD, Bean JC, Lin TW, Sathyamurthy A, Xiong WC, *et al.* Regulation of spine formation by ErbB4 in PV-positive interneurons. J Neurosci 2013, 33: 19295–19303.
36. Harris KM, Stevens JK. Dendritic spines of CA 1 pyramidal cells in the rat hippocampus: Serial electron microscopy with reference to their biophysical characteristics. J Neurosci 1989, 9: 2982–2997.
37. Rex CS, Chen LY, Sharma A, Liu J, Babayan AH, Gall CM, *et al.* Different Rho GTPase-dependent signaling pathways initiate sequential steps in the consolidation of long-term potentiation. J Cell Biol 2009, 186: 85–97.
38. Huang L, Li Q, Wen R, Yu Z, Li N, Ma L, *et al.* Rho-kinase inhibitor prevents acute injury against transient focal cerebral ischemia by enhancing the expression and function of GABA receptors in rats. Eur J Pharmacol 2017, 797: 134–142.
39. Liley AW. The quantal components of the mammalian end-plate potential. J Physiol 1956, 133: 571–587.
40. Del CJ, Katz B. Potential and resistance changes at the motor endplate. J Physiol 1954, 123: 70P–71P.
41. Habets RL, Borst JG. Dynamics of the readily releasable pool during post-tetanic potentiation in the rat calyx of Held synapse. J Physiol 2007, 581: 467–478.
42. Tang Y, Zucker RS. Mitochondrial involvement in post-tetanic potentiation of synaptic transmission. Neuron 1997, 18: 483–491.
43. Kang S, Ling QL, Liu WT, Lu B, Liu Y, He L, *et al.* Down-regulation of dorsal striatal RhoA activity and impairment of working memory in middle-aged rats. Neurobiol Learn Mem 2013, 103: 3–10.
44. Rozic G, Lupowitz Z, Piontkewitz Y, Zisapel N. Dynamic changes in neurexins' alternative splicing: Role of Rho-associated protein kinases and relevance to memory formation. PLoS One 2011, 6: e18579.
45. Sanders SJ, Ercan-Sencicek AG, Hus V, Luo R, Murtha MT, Moreno-De-Luca D, *et al.* Multiple recurrent de novo CNVs, including duplications of the 7q11.23 Williams syndrome region, are strongly associated with autism. Neuron 2011, 70: 863–885.
46. Kirov G, Pocklington AJ, Holmans P, Ivanov D, Ikeda M, Ruderfer D, *et al.* De novo CNV analysis implicates specific abnormalities of postsynaptic signalling complexes in the pathogenesis of schizophrenia. Mol Psychiatry 2012, 17: 142–153.
47. Meziane H, Khelfaoui M, Morello N, Hiba B, Calcagno E, Reibel-Foisset S, *et al.* Fasudil treatment in adult reverses behavioural changes and brain ventricular enlargement in Oligophrenin-1 mouse model of intellectual disability. Hum Mol Genet 2016, 25: 2314–2323.